مجلة الدراسات التربوية والعلمية - كلية التربية - الجامعة العراقية
العدد الرابع والعشرون - المجلد الرابع - علوم الكيمياء - تشرين ثاني 2024 م
doi.org/10.52866/esj.2023.04.24.21

Synthesis, Characterization and Studies on Thermal, Antioxidant, Docking and Biological of New Ligands with Some Metal Complexes

*Mohammed A. Mudhi , **Enass J. Waheed and *Maha Salih Hussein
* Department of Chemistry, College of Education, University of Samarra, Samarra, Iraq.
** Department of Chemistry, College of Education for Pure Sciences- Ibn -Al-Haitham, University of Baghdad, Baghdad, Iraq.
Corresponding author Email: enass.j.w@ihcoedu.uobaghdad.edu.iq
https://orcid.org/0000-0002-4051-0107

Abstract :

In the present work, metal complexes of Ni(II), Mn(II), Cu(II), Co(II), Zn(II), Cd(II) and Hg(II) had been synthesized with the use of new Ligands N1,N4-bis((1,5-dimethyl-3oxo-2phenyl-2,3dihydro-1H-pyrazol-4yl) carbamothioyl) succinamide (La) and N1,N4-bis ((4-(N-(5-methyl isoxazol- 3yl) sulfamoyl) phenyl) carbamothioyl) succinamide (Lb) derived from succinyl chloride with 4-aminoantipyrine and Sulfamethoxazole respectively. In comparison to standard antioxidants (ascorbic acid), their antioxidant activity against DPPH (1.1-Di-phenyl-2-picrylhydrazyl) will be assessed. According to the findings, when compared to the ascorbic acid standard reference, the zinc complex is more potent as an antioxidant compared to the nickel complex. With the use of the Autodock 4.2 tool, the hit compounds (La, Lb) were submitted to a docking study on glucosamine-6-phosphate synthase (GlcN-6P), molecular target enzyme for antimicrobial drugs. The most select compounds have been docked into GlcN-6-P. Orthosteric (active) site of the enzyme was found to bind to every hit, suggesting that a competitive inhibition mechanism may be at work. FT-IR, UV-visible, 1HNMR, 13CNMR, CHNS, TG, conductivity, and magnetic susceptibility have all been used to exanimate and confirm compounds. Tetrahedral geometry was proposed for all compounds of [M2(LaorLb)Cl4]. Additionally, anti-bacterial activity of ligands (La & Lb) and their complexes against two gram-positive and gram-negative bacteria types, including S. aureas and E. coli, was tested for the DMSO solution.

Key Words: Metal complexes, Sulfamethoxazole, 4-aminoantipyrine.

تحضير وتشخيص ودراسات على التفاعلات الحرارية ومضادات الأكسدة والالتحام والفعالية البيولوجية لليكاندات الجديدة مع بعض المعقدات الفلزية

*محمد احمد مضحي , **ايناس جاسم وحيد , *مها صالح حسين
*قسم الكيمياء, كلية التربية, جامعة سامراء, سامراء, العراق
**قسم الكيمياء, كلية التربية للعلوم الصرفة - ابن الهيثم ,جامعة بغداد, بغداد, العراق

مستخلص:

في العمل الحالي، تم تحضير المعقدات الفلزية Ni (II)، Mn (II)، Cu (II)، Co (II)، Zn (II)، Cd (II) وHg (II) باستخدام N1,N4-bis((1,5-dimethyl-3oxo-2phenyl-2,3dihydro-1H-pyrazol-4yl) carbamothioyl) succinamide (La) N1,N4-bis ((4-(N-(5-methyl isoxazol- 3yl) sulfamoyl) phenyl) carbamothioyl) succinamide (Lb) الليكاندات الجديدة المشتقة من كلوريد السكسينيل مع 4-أمينوأنتيبيرين وسولفاميثوكسازول على التوالي. بالمقارنة مع مضادات الأكسدة القياسية (حامض الأسكوربيك)، سيتم تقييم نشاطها المضاد للأكسدة ضد DPPH (1.1-Di-phe-nyl-2-picrylhydrazyl) وفقاً للنتائج، بالمقارنة مع المرجع القياسي حامض الأسكوربيك، فإن معقد الخارصين أكثر فعالية كمضاد للأكسدة مقارنة بمعقد النيكل.

باستخدام أداة Autodock 4.2،تم تقديم الليكاندات (La, Lb) إلى دراسة الالتحام الجزيئي على glucos-amine-6-phosphate synthase (GlcN-6P)، وهو إنزيم الهدف الجزيئي للأدوية المضادة للميكروبات. تم دمج المركبات المحددة على (GlcN-6P) وجد أن الموقع الفعال للإنزيم يرتبط بكل موقع، مما يشير إلى احتمال وجود آلية تثبيط تنافسية. تم استخدام كل من الاشعة تحت الحمراء، الاشعة المرئية-فوق البنفسجية، الرنين النووي البروتوني، التحليل الدقيق للعناصر، التحليل الحراري، التوصيلية، والحساسية المغناطيسية لفحص المركبات وتأكيدها. تم اقتراح هندسة رباعية السطوح لجميع مركبات [M_2(La or Lb) Cl_4]. بالإضافة إلى ذلك، تم اختبار النشاط المضاد للبكتيريا للمركبات (La & Lb) ومعقداتهما ضد نوعين من البكتيريا إيجابية الجرام وسالبة الجرام، بما في ذلك S. aureas and E. coli في مذيب DMSO.

الكلمات المفتاحية: المعقدات الفلزية ، سلفاميثاكسازول ، 4- امينوانتيبايرين .

Introduction

A certain anti-microbial substance class working against the bacteria is antibiotic. The antibiotic drugs are often utilized in prevention and treatment of bacterial infections since they're the most effective anti-bacterial agent type for doing so. They could stop bacterial growth (1,2). Bacteriostatic antibiotic sulfamethoxazole is frequently used to treat a number of infections. Both veterinary and human medicine frequently prescribe and use the antibiotic sulfamethoxazole (SMX). Numerous SMX derivatives have been produced, described, evaluated, and utilized to treat a variety of infections recently. Many SMX derivatives are presently being developed depending on heterocyclic moieties. They're utilized extensively in the clinical medicine and play the role of pharmacological agents with various biological procedures, including antiviral agents, cancer treatment, herbicidal activities, antifungal, antimycobacterial and antitubercular uses [3,4].

One of heterocyclic compounds having 2N atoms in their ring, connected with highly reactive amine, and carbonyl functional groups is 4-Aminoantipyrine. The presence of hetero atoms influences how electrons are distributed, resulting in the aromatic character that is known as the heteroatom effect, which also adds reactivity, chelating action, etc. As a result, it is helpful individually in the research fields like analytical, contemporary organic, bio-organic, and medicine chemistry. One of the pyrazole derivatives is 4-aminoantipyrine, an antipyretic drug. (5,6). The antibacterial, antioxidant, antifungal, tuberculostatic, insecticidal, and acaricidal properties of ligands containing sulphur are well recognized. Metals hold a prestigious position in medical chemistry. Their d-shells are filling up right now. Coordination complexes were established as a result of this feature of transition metals. A metal complex, also known as a coordination compound, is a structure that is made up of a central metal atom that is bound to a variety of molecules or anions (ligands) around it [7,8].

Generally, ligand antioxidants and their complexes operate as electron or hydrogen donors in an interaction site for neutralizing free radicals. The effectiveness of different organic com-

pounds at scavenging free radicals could be assessed using the DPPH and ABTS+ tests. It has already been discovered that various organic compounds have excellent antioxidant properties, thus it is critical to comprehend how such antioxidants work and how effective they are (9). The enzyme (GlcN-6P synthase) catalyzes iosynthesis of (GlcN-6P) from (Fru-6P) and glutamine as ammonia source, resulting in the production of (UDP-GlcNAc), which is necessary for molecular docking. The development of amino sugar macro-molecule units, essential for the synthesis of the cell wall of a micro-organism, depends on such biosynthetic reaction cascades. Fig. (10) depicts the target enzyme's binding pocket, which contains the amino acid residues Gly 301, Ser 303, Thr 302, Ser 347, Cys 300, Thr352, Ser 349, Val 399, Gln 348, Ser401, Ala 602, and Lys603.

In the presented work, seven complexes of each ligand—L^a and L^b—are synthesized and characterized. They are produced via reactions of succinyl chloride with 4-aminoantipyrine and sulfamethoxazole, respectively, and transition metal ions like Ni(II), Mn(II), Cu(II), Co(II), Cd(II), and Zn(II) and Hg(II).

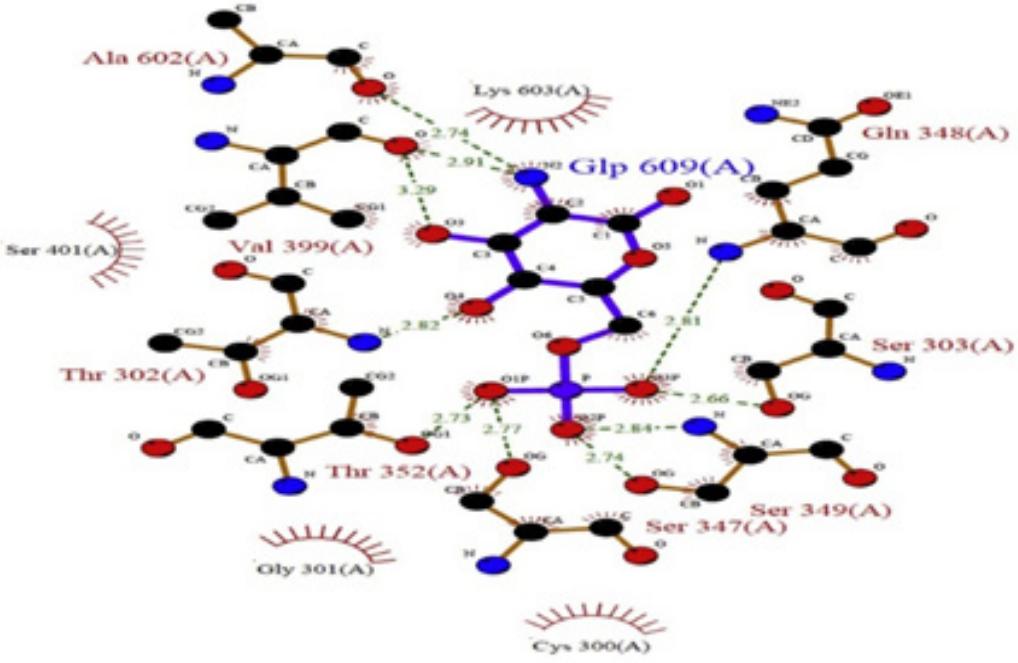

Fig1. 2-D diagram of molecular target enzyme; (GlcN-6P) with its physiological ligand glucosamine-6-phosphate binding in active site.

2. Materials and Methods

2.1. General

The (L^a & L^b) as well as their complexes were synthesized using only pure grade reagents and chemicals, which were obtained from Fluka, BDH, and Merck chemical companies. The device (Shimadzu 8400s FT-IR) and CsI disc were used for measuring infrared spectroscopy within the range (200-4000 cm^{-1}). The melting point of compounds that have been synthesized in open tube has been measured by using electro-thermal melting point device (SMP-10 Stuart). Electron spectra of produced compounds have been examined with the use of a (Shimadzu UV1800) visible ultra-violet spectrophotometer with 10^{-3}M samples concentration in DMSO solvent at the temperature of the room and quartz cell of 1cm length. Chemical displacements in the (NMR spectra ^1H & ^{13}C) in (DMSO-d6 with TMS) were acquired with the use of (Bruker 300 MHz NMR spectrometer). %M in complexes is calculated using a Shimadzu (AA 680) device. Molar conductivity of synthesized compounds was measured at room temperature with the use of a device (Philips pw-Digital conductivity meter) at concentration of (10^{-3}M) in (DMSO). (μeff B.M) of complexes have been measured at room temperature with the use of a device (magnetic sensitivity balance (Sherwood Scientific)). The prepared compounds' (%M, %C, %H, %N, %S) were calculated by using a device called the Euro EA 300. TGA has been carried out with the use of an STA PT1000 Linseis and argon gas, at temperatures between 0 and 1000 °C.

2.2. Chemistry

2.2.1. Synthesis of ligands (L^a or L^b) [11,12]

-The step A

Potassium thiocyanate (0.25g, 2.57mmol) was dissolved in dry acetone (20.0ml). The first solution was given a gradual addition of succinyl chloride (0.14ml, 0.2g, 1.3mmol) while being stirred at room temperature for an hour. Potassium chloride was removed from the white precipitate.

-The step B

4-Aminoantipyrine or SMX (0.51 g, 2.5mmol) or (0.63g, 2.5 mmol) are dissolved in dry acetone (15ml), added, and stirred into the solution obtained in step A. This solution is after

that refluxed at a 50°–55°C temperature for three–five hrs. After this solution had been at room temperature for 1hr, ice powder has been added, and the bottle was left with mixture until precipitate had been formed. Good production (72% or 63%, according on Scheme1).

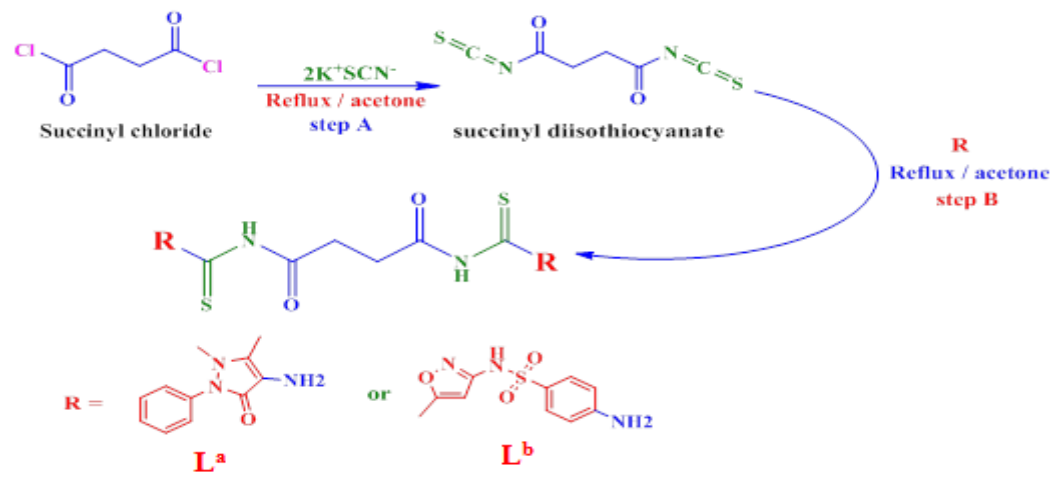

Scheme1: Preparation course of the Ligands (L^a & L^b)

2.2.2. Synthesis of complexes

- Synthesis of $[Cu_2(L^a \text{ or } L^b)Cl_4]$ complex:

Complexes have been made in the following molar ratios: (M: L^a or L^b) (2: 1). Ethanol solution (10 ml) of the ligand (L^a or L^b) (0.1gm, 0.16mmol) or (0.1gm, 0.16mmol) was combined with the metal chloride ($CuCl_2.2H_2O$) (0.06gm, 0.32mmol). This mixture has been kept at 70 °C for 3–4 hrs while being constantly stirred and reflexed. Each ligand's color (olive) generated a precipitate. The precipitate has been filtered, washed with distilled water and diethyl ether numerous times, and then crystallized again with 100% ethanol.

- Synthesis of $[M_2(L^a \text{or} L^b)Cl_4]$ complexes

The procedure utilized to make such complexes was comparable to that used to make compound [Cu2(L^a or L^b)Cl_4] in the paragraph above. The precipitate of Ni (II), Co (II), Cd (II), Mn (II), and Hg (II) complexes had been obtained and washed numerous times with the distilled water and diethyl ether before being re-crystallized with the absolute ethanol, can be seen from scheme (2).

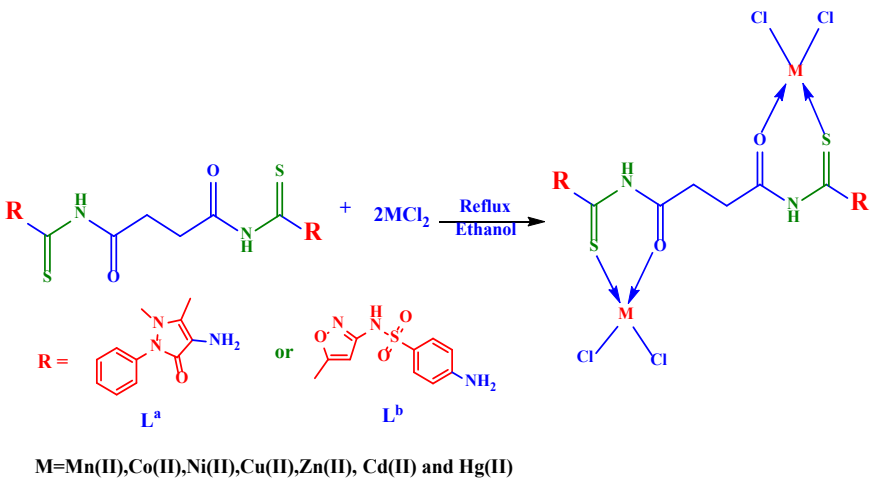

Scheme2: Preparation route of complexes $[M_2(L^a \text{or } L^b)Cl_4]$

3. Results and Discussion

The prepared metal complexes' most crucial properties include their thermal stability and the makeup of colored solid. Soluble in DMF and DMSO as solvents. All prepared complexes' theoretical and practical (A.A) measurements were estimated; see Tables (1-A) and (1-B).

Table (1-A): Different physical properties of (L^a) as well as its complexes

Com.	M.wt g / mol	m.p°C or dec.	colour	Microanalysis found (calc.) %					
				M	C	H	N	S	Cl
L^a	606.72	172-174	Orange	------	55.45 (55.43)	4.96 (4.98)	18.49 (18.47)	10.53 (10.57)	------
$[Mn_2(L^a)Cl_4]$	858.40	188-190	Light orange	12.82 (12.80)	39.20 (39.18)	3.54 (3.52)	13.12 (13.05)	7.51 (7.47)	16.56 (16.52)
$[Co_2(L^a)Cl_4]$	866.39	168-170	Dark blue	13.62 (16.04)	38.88 (29.98)	3.53 (3.36)	12.97 (19.34)	7.42 (7.40)	16.41 (8.96)
$[Ni_2(L^a)Cl_4]$	865.91	184-186	Green	13.64 (13.56)	38.87 (38.84)	3.51 (3.49)	12.93 (12.94)	7.49 (7.40)	16.43 (16.38)
$[Cu_2(L^a)Cl_4]$	875.61	168-170	Olive	14.57 (14.51)	38.43 (38.41)	3.42 (3.45)	12.87 (12.80)	7.35 (7.32)	16.23 (16.19)
$[Zn_2(L^a)Cl_4]$	879.28	176-178	Light orange	14.81 (14.87)	38.27 (38.25)	3.46 (3.44)	12.78 (12.74)	7.31 (7.29)	16.15 (16.13)
$[Cd_2(L^a)Cl_4]$	973.34	>300	Light orange	23.12 (23.10)	34.57 (34.55)	3.15 (3.11)	11.53 (11.51)	6.62 (6.59)	14.60 (14.57)
$[Hg_2(L^a)Cl_4]$	1149.70	184-186	Light orange	34.92 (34.89)	29.28 (29.25)	2.66 (2.63)	9.78 (9.75)	5.59 (5.58)	12.36 (12.33)

Table (1-B): Different physical properties of (L^b) as well as its complexes

Com.	M.wt g / mol	m.p°C or dec.	colour	Microanalysis found % (.calc)					
				M	C	H	N	S	Cl
L^b	706.78	180-182	Or-ange	-------	44.21 (44.18)	3.73 (3.71)	15.87 (15.85)	18.16 (18.14)	-------
$[Mn_2(L^b)Cl_4]$	958.46	300>	Off white	11.45 (11.46)	32.52 (32.58)	2.75 (2.73)	11.72 (11.69)	13.41 (13.38)	14.84 (14.79)
$[Co_2(L^b)Cl_4]$	966.45	128-130	Dark blue	12.23 (12.20)	32.37 (32.31)	2.73 (2.71)	11.63 (11.59)	13.23 (13.27)	14.65 (14.67)
$[Ni_2(L^b)Cl_4]$	965.97	162-164	Green	12.17 (12.15)	32.38 (32.33)	2.79 (2.71)	11.63 (11.60)	13.29 (13.28)	14.64 (14.68)
$[Cu_2(L^b)Cl_4]$	975.67	300>	Olive	13.13 (13.03)	32.07 (32.01)	2.65 (2.69)	11.44 (11.48)	13.11 (13.14)	14.55 (14.53)
$[Zn_2(L^b)Cl_4]$	979.34	172-174	Light orange	13.38 (13.35)	31.83 (31.89)	2.62 (2.68)	11.46 (11.44)	13.11 (13.09)	14.51 (14.48)
$[Cd_2(L^b)Cl_4]$	1073	300>	Light orange	20.91 (20.94)	29.03 (29.09)	2.47 (2.44)	10.43 (10.44)	11.91 (11.95)	13.26 (13.21)
$[Hg_2(L^b)Cl_4]$	1249.76	178-180	Light orange	32.13 (32.10)	24.96 (24.99)	2.13 (2.10)	8.93 (8.97)	10.29 (10.26)	11.38 (11.35)

3.1. Mass spectra

The mass spectral data fragmentation of (L^a), Fig.(2) showed ((M^+=606.7) (20%) and chemical formula [$C_{28}H_{30}N_8O_4S_2$] [13]. While data fragmentation of the mass spectra of L^b, Fig. (3) showed (M^+=706.7) (36.76%) and chemical formula [$C_{26}H_{26}N_8O_8S_4$] [14]. Additional fragmentation are displayed in Table (2),Scheme (3,4).

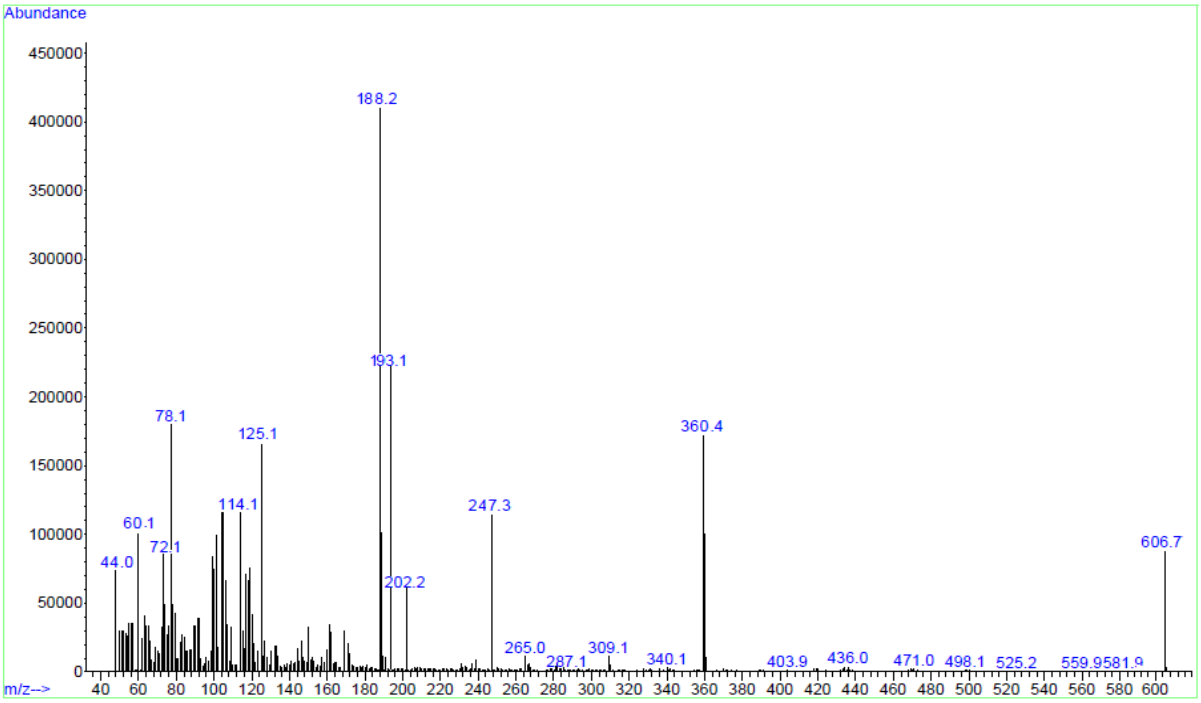

Fig. (2): Mass spectrum regarding L^a.

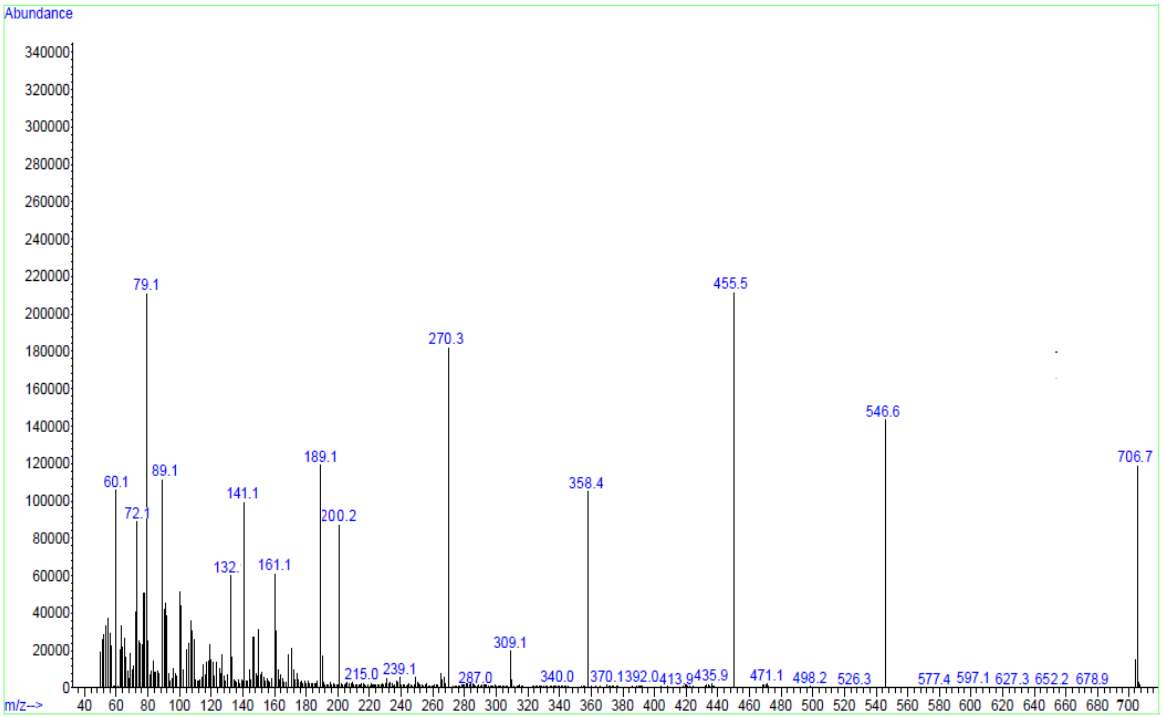

Fig. (3): Mass spectrum regarding L^b.

Table (2): Fragmentation of mass spectrum regarding (L^a and L^b)

Fragment ligand (L^a)	Mass/charge (m/z)	Fragment ligand (L^b)	Relative Abundance (%)	Mass/charge (m/z)	Relative Abundance (%)
$[C_{28}H_{30}N_8O_4S_2]^{\cdot+}$	606.72	$[C_{26}H_{26}N_8O_8S_4]^{\cdot+}$	20	706.78	36.76
$[C_{16}H_{18}N_5O_3S]^{\cdot+}$	360.41	$[C_{22}H_{22}N_6O_5S_3]^{\cdot+}$	40	546.64	45.59
$[C_{12}H_{13}N_3O_5]^{\cdot+}$	247.32	$[C_{16}H_{17}N_5O_5S_3]^{\cdot+}$	25.56	455.52	64.71
$[C_{11}H_{12}N_3O]^{\cdot+}$	202.25	$[C_{12}H_{12}N_3O_4S_3]^{\cdot+}$	14.45	358.43	5.88
$[C_5H_7N_3O_2S]^{\cdot+}$	193.17	$[C_{10}H_{10}N_2O_3S_2]^{\cdot+}$	50	270.32	55.88
$[C_{11}H_{12}N_2O]^{\cdot+}$	188.23	$[C_7H_6NO_2S_2]^{\cdot+}$	91	200.25	25
$[C_5H_7N_3O]^{\cdot+}$	125.13	$[C_4H_5N_2O_3S]^{\cdot+}$	36.67	161.16	19.12
$[C_4H_6N_2O_2]^{\cdot+}$	114.10	$[C_6H_5O_2S]^{\cdot+}$	25.56	141.16	29.41
$[C_6H_6]^{\cdot+}$	78.11	$[C_2H_3NO_5]^{\cdot+}$	41.12	89.11	33.82
$[C_3H_6NO]^{\cdot+}$	72.09	$[C_3H_6NO]^{\cdot+}$	18.89	72.09	27.94
$[CH_2NS]^{\cdot+}$	60.09	$[CH_2NS]^{\cdot+}$	22.23	60.09	32.35
$[CH_2NO]^{\cdot+}$	44.03	$[C_{26}H_{26}N_8O_8S_4]^{\cdot+}$	16.67	706.78	36.76
		$[C_{22}H_{22}N_6O_5S_3]^{\cdot+}$		546.64	45.59
		$[C_{16}H_{17}N_5O_5S_3]^{\cdot+}$		455.52	64.71

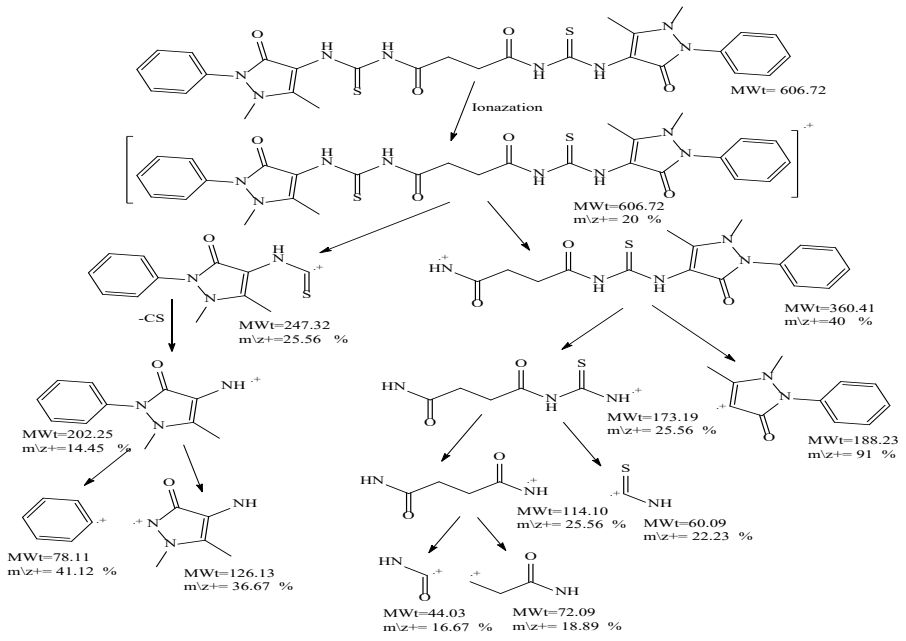

Scheme (3): Expected fragmentation in the ligand (L^a) spectrum

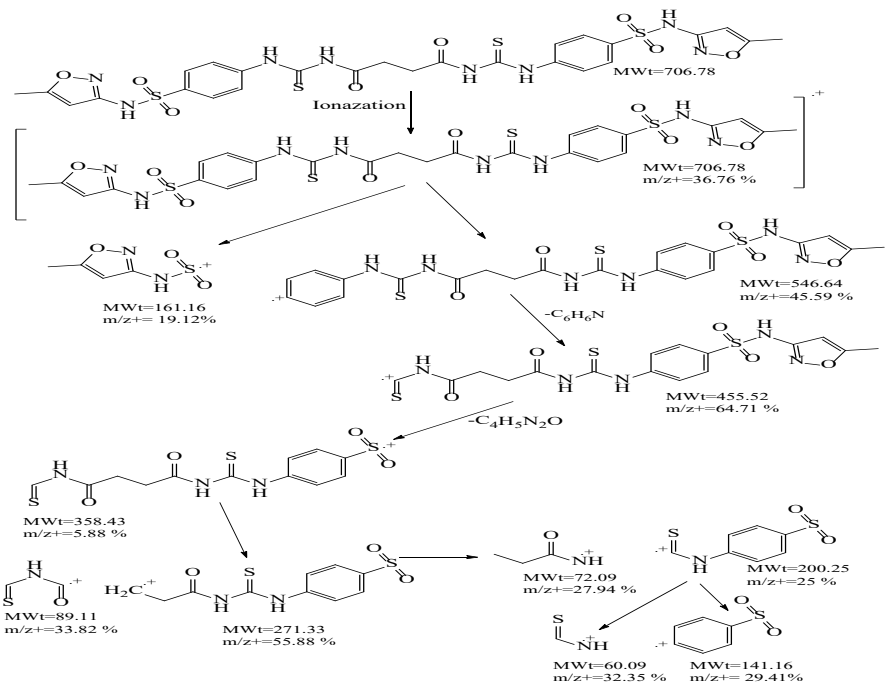

Scheme (4): Expected fragmentation in the ligand (L^b) spectrum

3.2. NMR Spectra

3.2.1. ^{1}H-NMR Spectra of (L^a and L^b)

An integrated intensity of each signal in the ^{1}HNMR spectra of ligands (L^a and L^b) has been consistent with the number of various groups of protons present [15-18], as listed in the Table3.

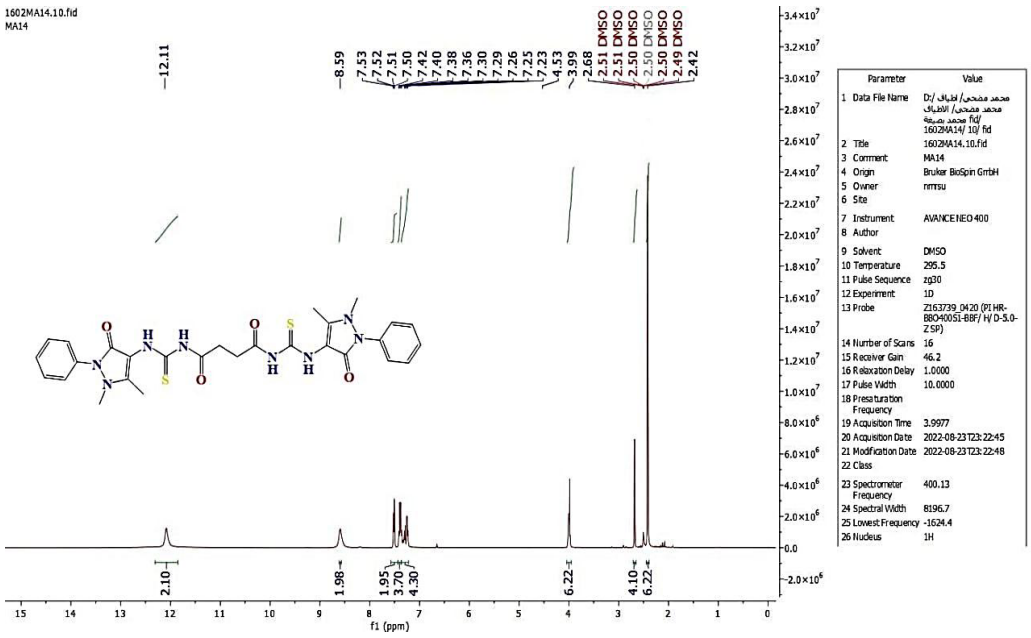

Fig4: ^{1}H-NMR spectrum regarding L^a

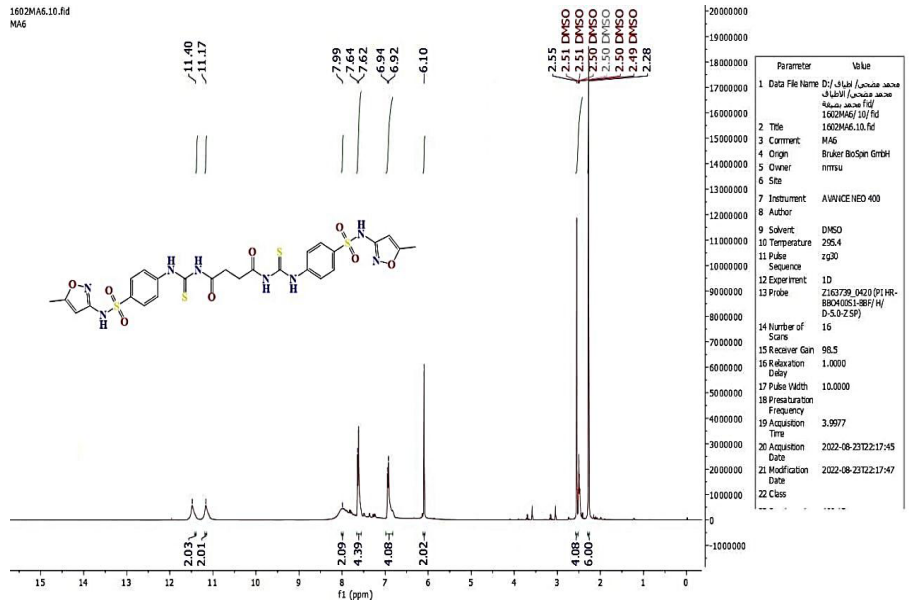

Fig5: ^{1}H-NMR spectrum regarding L^{b}

Table (3): ^{1}H-NMR data for (L^{a} and L^{b}) measured in DMSO-d^{6} as well as chemical shift in ppm

Ligands	Protons kind	δ (ppm)	Ligand	Protons kind	δ (ppm)
L^{a}	2 H (singlate), proton CSN**H** group	12.11	L^{b}	2 H (singlate), proton CSN**H** group	11.40
	2 H (singlate), proton CON**H** group	8.59		2 H (singlate), proton CON**H** group	11.17
	10H (multiplate), proton aromatic (six ring) from antipyrine	7.23-7.53		2H (singlate), proton SO_2N**H** from Sulfamethoxazole	7.99
	6H (singlate), proton C**H**$_3$-N in (five ring) from antipyrine	3.99		4H (doublet), proton aromatic (six ring) from Sulfamethoxazole	7.62-7.64
	4 H (triplate), proton C**H**$_2$ group from methylene succinyl	2.68		4H (doublet), proton aromatic (six ring) from Sulfamethoxazole	6.92-6.94
	6 H (singlate), proton C**H**$_3$- C in (five ring) from antipyrine	2.42		2H (singlate), proton C**H** in (five ring) from Sulfamethoxazole	6.10
				4 H (triplate), proton C**H**$_2$ group from methylene succinyl	2.55
				6H (singlate), proton C**H**$_3$-C in (five ring) from Sulfamethoxazole	2.28

3.2.2. ^{13}C-NMR Spectra of (L^a and L^b)

In integrated intensity of each signal in the ^{13}CNMR spectra of ligands (L^a, L^b) was found to be consistent with the number of different groups of carbons presents [19-22], as listed in the Table (4)

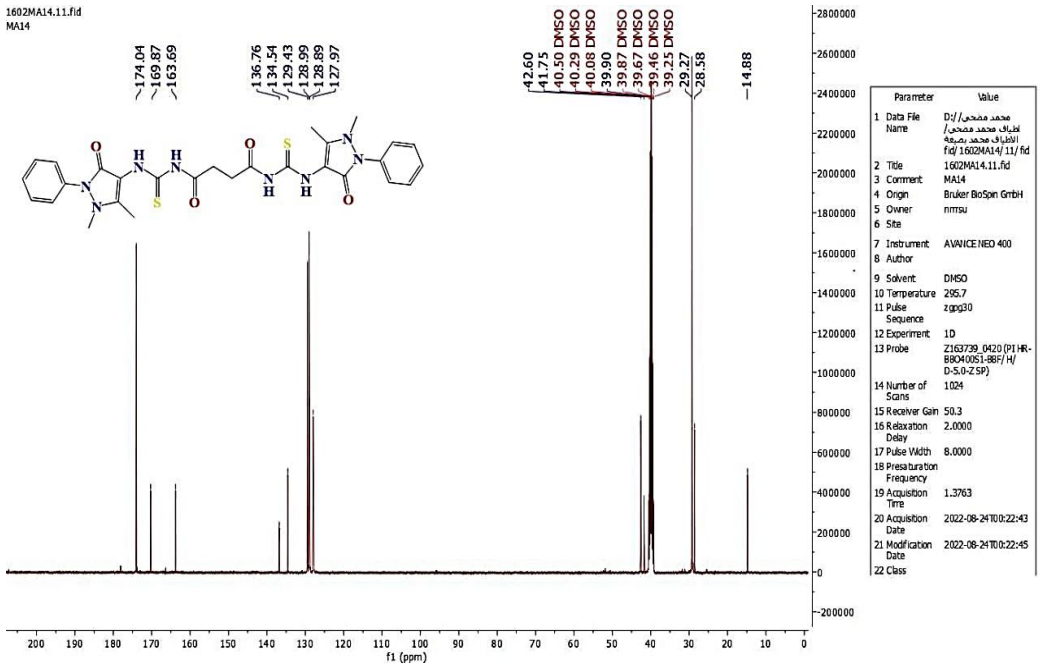

Fig. (6): ^{13}C-NMR spectrum regarding L^a

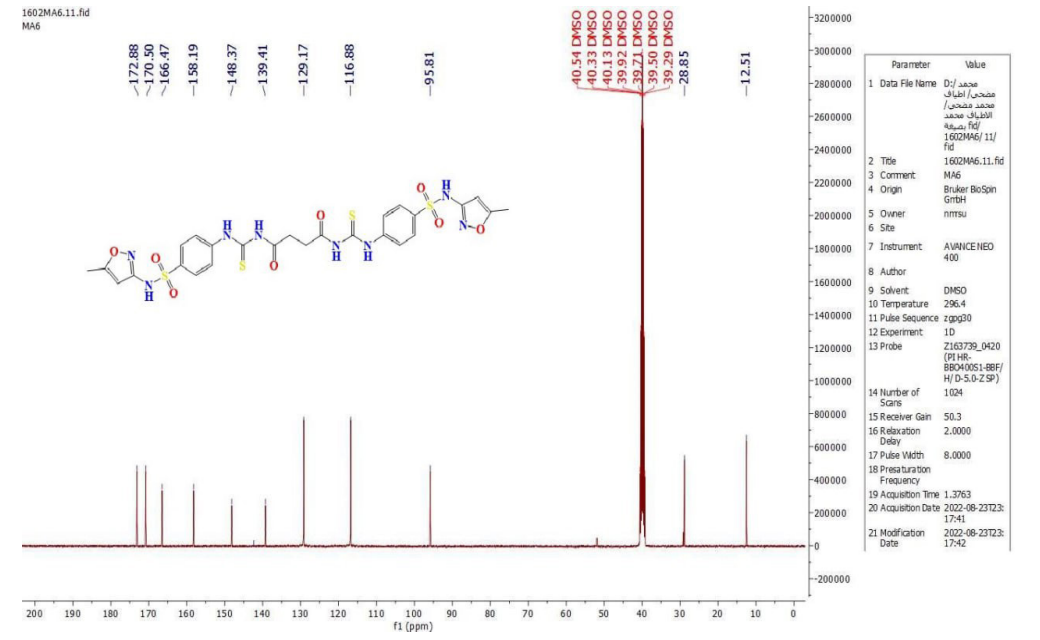

Fig. (7): ^{13}C-NMR spectrum regarding L^b

Table (4): ^{13}C-NMR data for (L^a and L^b) measured in the DMSO-d^6 as well as chemical shift in ppm

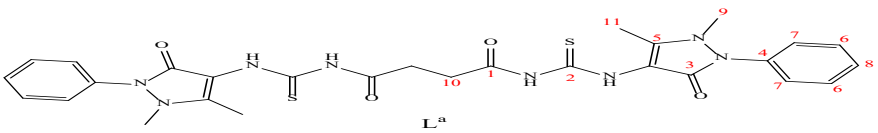

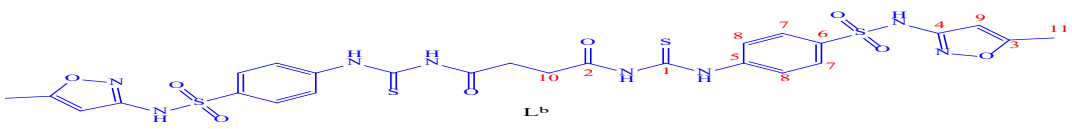

Ligands	Carbons kind	δ (ppm)	Ligand	Carbons kind	δ (ppm)
L^a	C_1 for C=O, amide group	174.04	L^b	C_1 for C=S, thioamide group	174.04
	C_2 for C=S, thioamide group	169.87		C_2 for C=O, amide group	169.87
	C_3 for C=O (in five ring), antipyrine group	163.69		C_3 for CO (five ring), Sulfamethoxazole group	163.69
	C_4 for phenyl (six ring), antipyrine group	136.76		C_4 for C=N (five ring), Sulfamethoxazole group	136.76
	C_5 for C-N in (five ring), antipyrine group	134.54		C_5 for phenyl (six ring), Sulfamethoxazole group	134.54
	$C_{6-}C_8$ for phenyl (six ring), antipyrine group	127.97-129.43		C_6 for phenyl (six ring), Sulfamethoxazole group	127.97-129.43
	C_9 for CH_3-N in (five ring), antipyrine group	39.90		C_7 for phenyl (six ring), Sulfamethoxazole group	127.97-129.43
	C_{10} for (CH_2-CH_2) aliphatic in succinyl group	29.27		C_8 for phenyl (six ring), Sulfamethoxazole group	127.97-129.43
	C_{11} for CH_3-C in (five ring), antipyrine group	14.88		C_9 for C=C (five ring), Sulfamethoxazole group	39.90
				C_{10} for (CH_2-CH_2) aliphatic in succinyl group	29.27
				C_{11} for CH_3-C, (five ring), Sulfamethoxazole group	14.88

3.3. The Fourier-transform infrared spectra

3.3.1. Ligand (L^a and L^b)

In addition to absorption bands at (1347 & 1168) cm-1 that had been determined to be (C=S), a different absorption band had shown at (1230cm-1) could be expressed as (C-N) (23), fig. (8). The two bands at (3413 and 3312cm-1) in La spectrum had been determined to (NH), whereas another absorption band had appeared at

(1721cm-1) could be expressed as υ(C=O) amide. The two band at (3456 & 3317) cm-1 in Lb spectrum determined to υ(NH), whereas another absorption band had emerged at (1739) cm-1 can be expressed as υ(C=O) amide, besides absorption bands at (1379 and 1165) cm-1 that had been determined to υ(C=S), and a different absorption band had emerged at (1267cm-1) can be expressed as υ(C-N) (24), Fig.(9).

3.3.2. Ligand (L^a and L^b) Complexes

Those spectra revealed a distinct variety of bands that belonged to the υ(CO, amide group) stretching vibration in region of (1697-1693) cm^{-1} that were shifted to different values of the frequency, suggesting likelihood of coordination of (L^a) by oxygen atom at amide group. Indicating that the sulfur atom was engaged in coordination, stretching vibration band υ(C=S) has been discovered in the region of (1342-1311) and (1177-1165) cm^{-1} moved to a new frequency. No variations in the group's set frequencies of (3483-3390) and (3394-3318) cm^{-1} in the complexes proved that the υ(N-H) in (La) has not been associated with the central ion. New bands υ(M-S, thioamide group), υ(M-O,amide group), and υ(M-Cl) in (489-459) cm^{-1}, (551-520 cm^{-1}, and (383-372) cm^{-1} ranges in ligand (La) were detected in the spectrum of the ligand complexes. Appearance of the new bands showing the formation of metal complexes was caused by coordination through sulfur atom in (NH-S=O) group, oxygen atom in (NH-C=O) group, and ion chloride (Cl-) [25–27]. Data from the FT-IR are shown in Table (5-A). The (La) and its complexes' spectra were shown in Fig. (8).

Those spectra revealed a distinct range of bands which belonged to stretching vibration of the υ(CO, amide group) in a range of (1720-1689) cm^{-1} that were shifted to different frequency values, suggesting a likelihood of (L^b) coordination by oxygen atom at amide group. Indicating that the sulfur atom has been involved in coordination, stretching vibration band υ(C=S) has been discovered in a range of (1396-1327) and (1176-1172) cm^{-1} moved to a new frequency. There were no variations in frequencies of this group, which have been set at (3491-3414) and (3402-3314) cm^{-1} in the complexes, indicating that the υ(N-H) in (L^b) has not been correlated with the central ion.

New bands υ(M-S, thioamide group), υ(M-O, amide group), and υ(M-Cl) in a (493-442), (574-559), and (384-322) cm^{-1} range in ligand (L^b) were detected in the spectrum of the ligand complexes. The appearance of new bands showing the creation of metal complexes was caused by coordination through sulfur atom in (NH-S=O) group, oxygen atom in (NH-C=O) group, and ion chloride (Cl-) (28,30). Table (5-B) presents the FT-IR data. The spectra of (L^b) and its complexes were shown in Fig. 9.

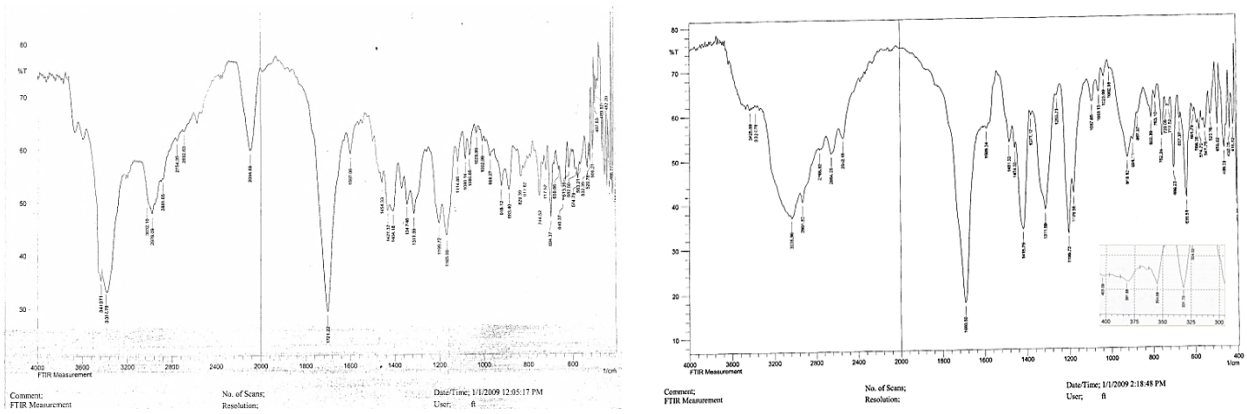

Fig. (8). L^a spectrum's FTIR as well as $[Cd_2(L^3)Cl_4]$

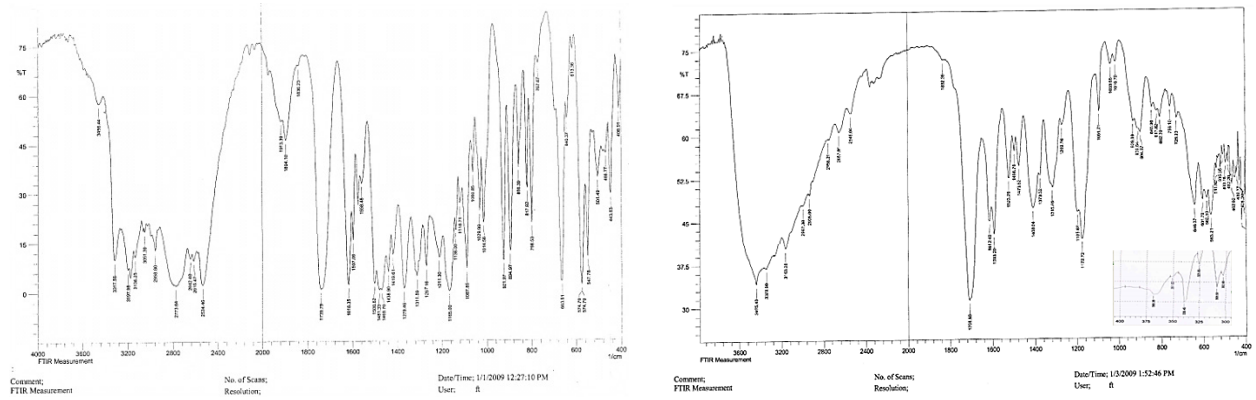

Fig. (9) L^b spectrum's FTIR as well as $[Cu_2(L^4)Cl_4]$

Table5-A: FT-IR data of (L^a) (cm^{-1}) as well as its complexes

Com.	(N-H)υ	(υC=O) Amide	υ(C=S) υ(C=S)	υ(C-N)	υ(M-O)	υ(M-S)	υ(M-Cl)
L^a	3413 3312	1721	1347 1168	1230	——	——	——
$[Mn_2(L^a)Cl_4]$	3410 3387	1693	1330 1176	1257	524	489	320
$[Co_2(L^a)Cl_4]$	3411 3394	1697	1311 1176	1199	551	459	283
$[Ni_2(L^a)Cl_4]$	3490 3356	1693	1330 1176	1253	524	489	341
$[Cu_2(L^a)Cl_4]$	3441 3379	1697	1342 1165	1253	536	482	361
$[Zn_2(L^a)Cl_4]$	3483 3318	1693	1311 1176	1257	524	478	351
$[Cd_2(L^a)Cl_4]$	3425 3322	1693	1311 1176	1253	520	489	326
$[Hg_2(L^a)Cl_4]$	3470 3342	1693	1338 1177	1258	551	489	372

Table5-B: FT-IR data of (L^b) (cm^{-1}) as well as its complexes

Com.	(N-H)υ	(υC=O) Amide	υ(C=S) υ(C=S)	υ(C-N)	υ(M-O)	υ(M-S)	υ(M-Cl)
L^b	3456 3317	1739	1379 1165	1267	——	——	——
$[Mn_2(L^b)Cl_4]$	3433 3375	1708	1369 1176	1269	563	489	384
$[Co_2(L^b)Cl_4]$	3414 3314	1708	1327 1176	1269	567	470	365
$[Ni_2(L^b)Cl_4]$	3491 3402	1720	1396 1172	1273	574	442	331
$[Cu_2(L^b)Cl_4]$	3476 3378	1708	1373 1172	1269	563	493	322
$[Zn_2(L^b)Cl_4]$	3468 3329	1708	1373 1176	1261	559	462	367
$[Cd_2(L^b)Cl_4]$	3456 3375	1689	1396 1176	1285	563	493	372
$[Hg_2(L^b)Cl_4]$	3475 3375	1708	1373 1176	1269	563	482	341

3.4. Electronic spectra

3.4.1. Ligands (L^a and L^b)

In the electronic spectrum of (La) (31), the largest absorption intensity has been discovered at (33670) cm-1, due to the transitions (π→π*), and at (28985) cm-1, which is due to transitions (n→π*). Fig.(10) data are provided in Table (6-A). In electronic spectrum of (Lb) (32), the maximum absorption intensities were reported at (37037) cm-1, which is attributable to transitions (π→π*), and at (32786) cm-1, due to the transitions (n→π*). The data from Fig. (11) are listed in Table (6-B).

3.4.2. Ligands (L^a and L^b) Complexes

Ligand (L^a) Complexes / electronic spectrum of Mn complex had shown bands at the values of (33557, 23529 and 12953) cm^{-1} because of LF, CT and $^6A_1 \rightarrow {}^4T_{2(G)}$ transitions respectively, which suggests that it had tetra-hedral geometry. On a basis of bands in Cobalt complex at the values of (33670, 22222, 14684 and 10905) cm^{-1}, which is back to the LF, LF, CT mix $^4A_{2(F)} \rightarrow {}^4T_{1(F)}$, $^4A_{2(F)} \rightarrow {}^4T_{1(P)}$ and $^4A_{2(F)} \rightarrow {}^4T_{2(F)}$ transitions respectively, tetra-hedral geometry of the complex had been suggested. Concerning Nickel complex, electron spectra appear absorption bands can be assigned to LF, CT $_{with}$ $^3T_1 \rightarrow {}^3T_{1(P)}$, $^3T_1 \rightarrow {}^3A_{2(F)}$ and $^3T_1 \rightarrow {}^3T_{2(F)}$ transition which exhibit in (33783, 27777, 12836 and 10989cm^{-1}) respectively. those bands characterization is an indication that this complex has tetra-hedral geometry. Which confirms that the tetrahedral geometry of Co complex is the appearance of bands at (33,444 and 11,111) cm^{-1} return to LF and $^2T_2 \rightarrow {}^2E$ transitions. Tetra-hedral geometry of Zinc complex had been suggested on a basis of band which had appeared at (33,783 & 29,411) cm^{-1} which returns to LF and CT. Based on bands in Mercury complex at (33,783 & 24,390) cm^{-1}, returning to LF and CT transitions respectively, tetra-hedral geometry of complex has been suggested. Tetra-hedral geometry of Cd complex had been suggested based on band which had appeared at (33,670 & 26,666) cm^{-1} that returns to LF and CT [33-35]. In Table6-A, U.V. data has been shown. In Fig10, spectra of (L^a) and its complexes have been shown.

Ligand (L^b) Complexes/ electronic spectrum of Mn complex had shown bands at (36,764 and 12,706) cm^{-1} because of LF, and $^6A_1 \rightarrow {}^4T_{2(G)}$ transitions respectively, which suggests the fact that it had tetra-hedral geometry. Based on bands in Co complex at (36630, 16286, 14727 & 11627) cm^{-1}, which is back to LF, $^4A_2 \rightarrow {}^4T_{1(P)}$, $^4A_{2(F)} \rightarrow {}^4T_{1(F)}$ and $^4A_{2(F)} \rightarrow {}^4T_{2(F)}$ transition respectively, tetra-hedral geometry of complex has been suggested [24]. Concerning Ni complex, electron spectra appear absorption bands can be assigned to the LF, CT mix $^3T_1 \rightarrow {}^3T_{1(P)}$, $^3T_1 \rightarrow {}^3A_{2(F)}$ and $^3T_1 \rightarrow {}^3T_{2(F)}$ transition that exhibit in (36630, 24691, 13698 and 10893) cm^{-1} respectively. those bands' characterization is an indication that the complex has tetra-hedral geometry. Which confirms that tetra-hedral geometry of Co complex is appearance of bands at (36231, 32258 and 11820) cm^{-1} return to LF, LF and $^2T_{2\,(F)} \rightarrow {}^2E$ transitions. Tetra-hedral geometry of Zinc complex has been suggested on a basis of band which had appeared at (36,101 and 26,041) cm^{-1} that returns to L.F and CT. based on bands in Mercury complex at (37,735 and 26,881) cm^{-1}, that return to LF and CT transitions respectively, tetra-hedral geometry of the complex has been proposed. Cd complex's tetra-hedral geometry has been proposed on a basis of the band which had appeared at (37,174 and 25,706) cm^{-1} which is back to LF and CT [36-38]. In Table6-B, UV data has been displayed. In Fig.(11) (L^b) spectra and its complexes have been shown.

Table6-A: UV-Vis data of (L^a) and its complexes.

Com.	Wave number		A	ε_{max} molar^{-1} cm^{-1}	Transitions	μ_{eff} B.M.	Conducts $Ohm^{-1}cm^2mol^{-1}$ in solvent (DMSO)
	nm	cm^{-1}					
L^a	297 345	33670 28985	1.218 0.500	1218 500	$\pi \rightarrow \pi^*$ $n \rightarrow \pi^*$	-	4.6
$[Mn_2(L^a)Cl_4]$	298 425 772	33557 23529 12953	1.993 0.686 0.020	1993 686 20	L.F C.T $^6A_1 \rightarrow {}^4T_{2(G)}$	6.46	3.5
$[Co_2(L^a)Cl_4]$	297 450 681 917	33670 22222 14684 10905	1.544 0.780 0.018 0.015	1544 780 18 15	L.F L.F C.T Mix $^4A_{2(F)} \rightarrow {}^4T_{1(F)}$ $^4A_{2(F)} \rightarrow {}^4T_{1(F)}$ $^4A_{2(F)} \rightarrow {}^4T_{2(F)}$	5.04	14
$[Ni_2(L^a)Cl_4]$	296 360 779 910	33783 27777 12836 10989	1.972 0.765 0.081 0.015	1972 765 81 51	L.F C.T Mix $^3T_1 \rightarrow {}^3T_{1(P)}$ $^3T_1 \rightarrow {}^3A_{2(F)}$ $^3T_1 \rightarrow 3T_{2(F)}$	4.12	22.7
$[Cu_2(L^a)Cl_4]$	299 900	33444 11111	1.652 0.013	1652 13	L.F $^2T_{2\,(F)} \rightarrow {}^2E$	2.46	12
$[Zn_2(L^a)Cl_4]$	296 340	33783 29411	1.638 0.097	1638 97	L.F C.T	0	14.7
$[Cd_2(L^a)Cl_4]$	298 375	33670 26666	2.227 0.082	2227 82	L.F C.T	0	18.9
$[Hg_2(L^a)Cl_4]$	296 410	33783 24390	2.188 0.097	2188 97	L.F C.T	0	16

Table 6-B: UV-Vis data of (L^b) and its complexes

Com.	Wave number		A	ε_{max} molar^{-1} cm^{-1}	Transitions	μ_{eff} B.M.	Conducts Ohm^{-1}cm^{-2}mol^{-1} in solvent (DMSO)
	nm	cm^{-1}					
L^b	270 305	37037 32786	1.989 0.490	1989 490	$\pi - \pi^*$ $n - \pi^*$	-	3.3
$[Mn_2(L^b)Cl_4]$	272 787	36764 12706	1.970 0.013	1970 13	L.F $^6A_1 \rightarrow {}^4T_{2(G)}$	6.31	7.4
$[Co_2(L^b)Cl_4]$	273 614 679 860	36630 16286 14727 11627	2.282 0.207 0.324 0.011	2282 207 324 11	L.F $^4A_2 \rightarrow {}^4T_{1(P)}$ $^4A_{2(F)} \rightarrow {}^4T_{1(F)}$ $^4A_{2(F)} \rightarrow {}^4T_{2(F)}$	4.78	6.6
$[Ni_2(L^b)Cl_4]$	273 405 730 918	36630 24691 13698 10893	1.183 0.029 0.019 0.039	1183 29 19 39	L.F C.T Mix $^3T_1 \rightarrow {}^3T_{1(P)}$ $^3T_1 \rightarrow {}^3A_{2(F)}$ $^3T_1 \rightarrow {}^3T_{2(F)}$	3.70	11.3
$[Cu_2(L^b)Cl_4]$	276 310 846	36231 32258 11820	1.608 0.460 0.010	1608 460 10	L.F L.F $^2T_{2\,(F)} \rightarrow {}^2E$	2.17	13.7
$[Zn_2(L^b)Cl_4]$	277 384	36101 26041	2.529 0.097	2529 97	L.F C.T	0	25.3
$[Cd_2(L^b)Cl_4]$	269 389	37174 25706	1.331 0.087	1331 87	L.F C.T	0	19.6
$[Hg_2(L^b)Cl_4]$	265 372	37735 26881	1.734 0.069	1734 69	L.F C.T	0	15.9

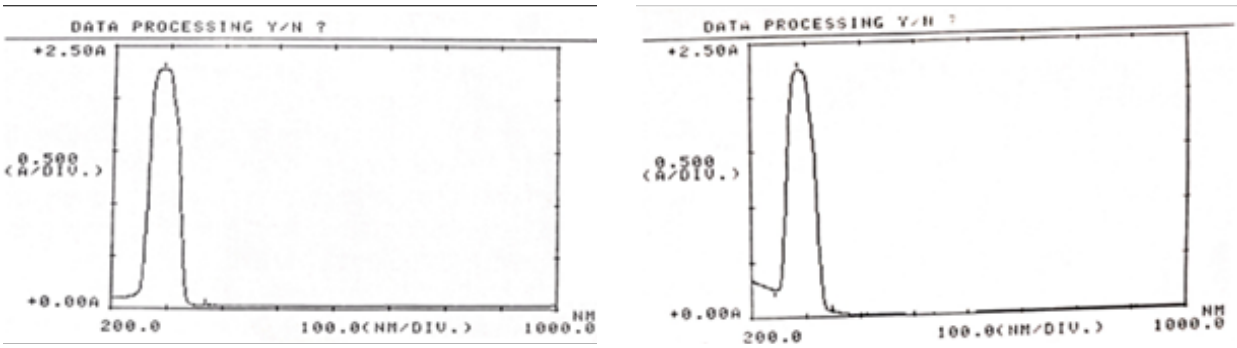

Fig. (10): Electronic spectrum of (L^a) and [$Hg_2(L^a)Cl_4$]

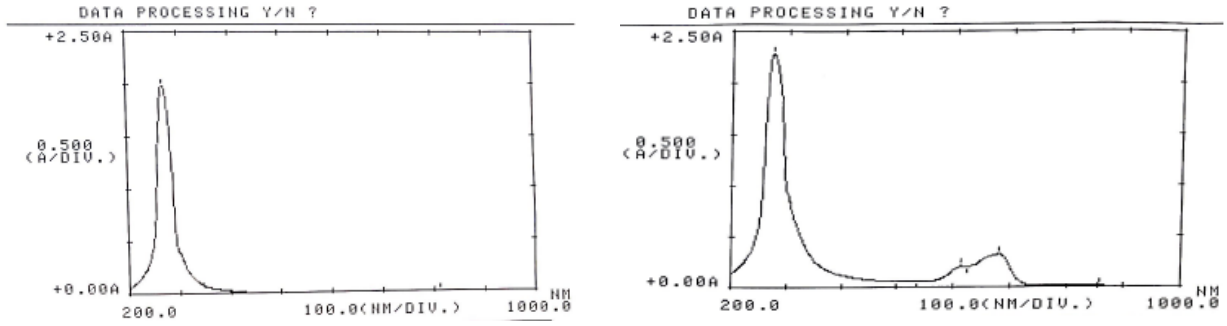

Fig. (11): Electronic spectrum of (L^b) and [$Co_2(L^b)Cl_4$].

3.5. Magnetic moments and Conductivity measurements

The measured values of the magnetic susceptibility and the effective magnetic moment (μeff) for complexes of Co(II), Mn (II), Ni(II), and Cu(II) have been shown in Tables (6-A and 6-B). These complexes have μeff values that are consistent with high spin tetrahedral complexes: 6.46, 5.04, 4.12, and 2.46 B.M. for La and 6.31, 4.78, 3.70, and 2.17 B.M. for Lb, respectively. All metal complexes were shown to be non-electrolytes based on molecular conductivity tests (39,40), Table (6-A and 6-B), and other sources.

3.6. Thermal analysis

With the use of a STAPT-1000 Linseis company1 Germany, the ligands (L^a and L^b) were synthesized and subjected to thermal analysis. This measurement was carried out in an argon gas atmosphere at a 10°C/min heating rate with 0–1000°C temperature range [41, 42]. Every result is taken from TG curves for those compounds that have been reviewed in Table7, Fig. (12) where it was reported.

Table7: Temperature degrees for the analyses in addition to corresponding values of weight loss.

ligands	Stage	TGA			DSC	
		T/°C range	%Estimated		T/°C	Peak
			Mass loss Found (Calc.)	Assignment		
L^a	1 2	50-280 281-600	1.813 (1.814) 2.285 (2.289)	$-2O_2$, $4N_2$, 2S, $9/2H_2$ -25C, $7H_2$	305.34 312.78	Exo. Endo.
L^b	1 2 3 + 4	50-100 101-255 256-600	0.2388(0.2456) 1.482(1.482) 1.1446(1.1620)	$-N_2$, O_2 $-3N_2$, $3O_2$, 4S, 4C, $3H_2$ -22C, $10H_2$	71.59 82.38 144.51 174.37 249.65 282.16	Endo. Exo. Exo. Endo. Endo. Exo.

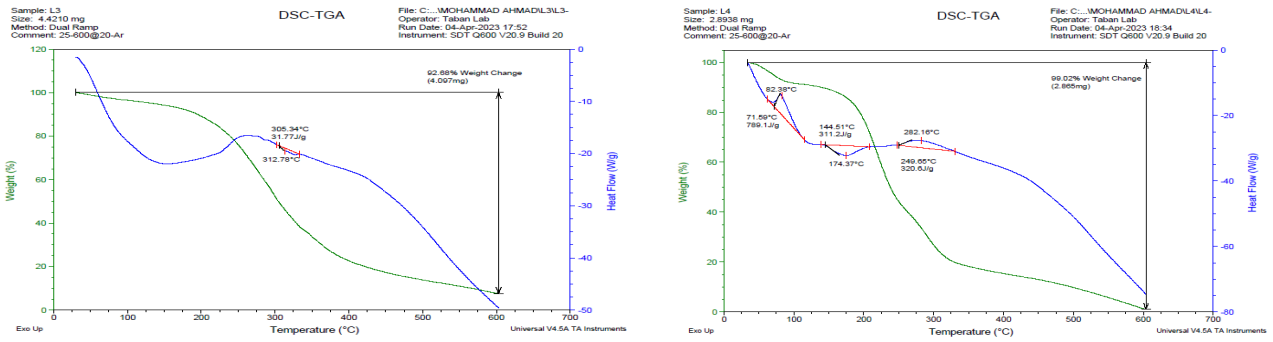

Fig. (12): Thermal study of (L^a and L^b)

3.7. Anti-microbial Activity Studies

Through measuring the inhibition zone in millimeters, newly synthesized compounds have been tested for the antibacterial activity with the use of the cupplate agar diffusion method. In a nutshell, Petri dishes were filled with sterilized agar media, which were then let to set. A sterilized triangular loop was used to disseminate microbial suspensions across the surface of the media. To bore cavities, a presterilized, 8 mm diameter stainless steel cylinder was employed. With the aid of a micropipette, all compounds under test were sequentially inserted into the cavities and given a one-hour diffusion peri-

od; pure DMSO served as the control. To test for antibacterial activity, these plates have been incubated at 37°C for 24 hrs. and 28°C for 48 hrs. Following the appropriate incubation, the inhibition zone around cups has been measured, and the compounds' percent inhibition was determined (43, 44). The data that were acquired are reported in Table8 and Fig13, 14.

Table8: The inhibition diameter values of (L^a & L^b) and theirs complexes.

No.	Com.	E. coli	Staphylococcus aureus
1	DMSO	0	0
2	L^a	5	13
3	L^b	15	8
4	D4 / $[Ni_2(L^b)Cl_4]$	12	**2**5
5	C7 / $[Hg_2(L^a)Cl_4]$	25	26

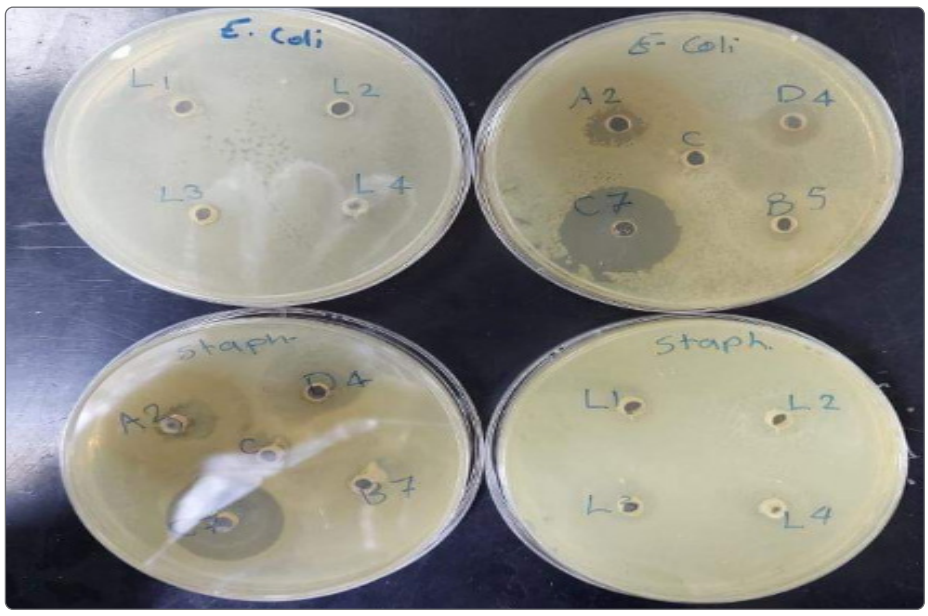

Fig13: diameters of inhibition of (L^a & L^b) and theirs complexes against certain bacteria

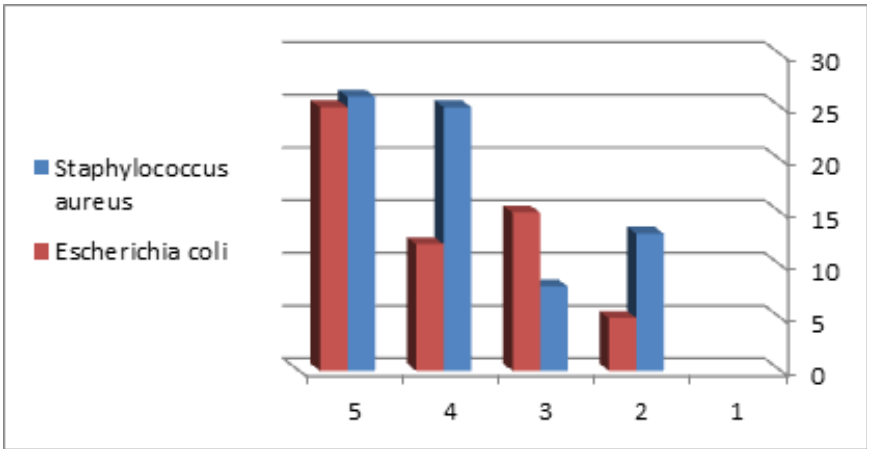

Fig14: Statistical representation for the microbial activities of the ligands and their complexes.

3.8. Antioxidant Test

DPPH free radical scavenging experiment was used to calculate the antioxidant potential. In a nutshell, 50 µl of DPPH solution was mixed with 30 µl of various compounds at concentrations ranging from 25 to 200 g, and the mix has then been incubated at room temperature for a duration of 30min in the dark. After 30 minutes, absorbance values are measured at 517nm by using ascorbic acid as a positive reference antioxidant activity. The % activity calculations are then performed, and it was shown that the zinc and nickel compounds were more active than the standard reference ascorbic acid. According to the findings, the zinc complex is a more potent antioxidant than the nickel complex when compared to ascorbic acid, the standard reference, as shown in Fig. (15), [45, 46], and Table (9).

Table (9): Antioxidant potential activity of compounds

Concentration µg mL^{-1}	Scavenging % (Mean±SD)		
	$[Ni_2(L^a)Cl_4]$	Vit.c	$[Zn_2(L^a)Cl_4]$
200	42.05±4.05	86.03±4.027	80.40±4.35
100	29.28±5.1	74.06±1.0	62.8±2.32
50	20.949±1.4	57.6±2.20	52.73±3.14
25	7.40±4.70	39±1.73	39.62±4.1

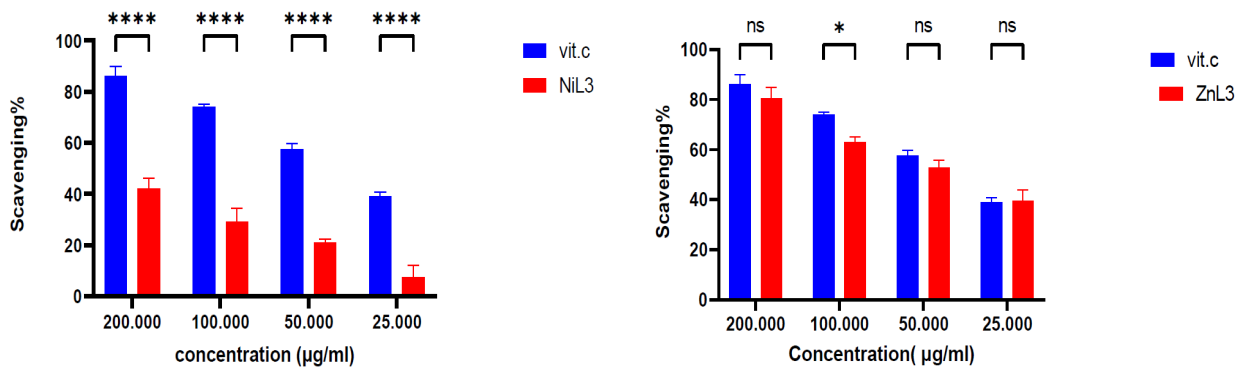

Fig. (15): antioxidant activity of nickel and zinc complexes compared to ascorbic acid as reference

2.4. Docking Study

The affinity of the two most powerful compounds (La, Lb) to GlcN-6P synthase binding site was examined using Auto Dock 4.2 bundle software. Protein Data Bank (PDB code 1-MOQ) provided PDB file construction of enzyme as target, which has been employed as a static structure. The protein residues were treated with hydrogen atoms after water was recovered, the natural ligand was eliminated, and the protein. The 2D structures of tested hits were created with the use of Chem Draw Ultra 7.0 and converted into mol for matted files with the use of open Babel 2.3.1 software. The grid of 62°A was formed on the enzyme's catalytic site's center during docking, with points spaced apart by 0.358 ˚A and designated as 30.5, 17.5, and -2.2 in X, Y, and Z, respectively. The docking algorithm was Lamarckian Genetic, with ten runs and 150 population sizes. The greatest number of energy evaluations—2.5 × 105, 27 × 103, and generations—were optimized by default.

One of the most well-liked methods for examining the binding affinity of small compounds in binding pocket of a protein with a known 3-D structure is the docking approach. The most powerful in vitro compounds (L^a, L^b) were put through docking research to

examine their binding affinity toward GlcN-6P synthase, which is the current compounds' molecular target. The Autodock 4.2 tool's Lamarckian Genetic Algorithm (LGA) was utilized in order to execute the docking. Based on the top four conformers that displayed best percent inhibition constant (Ki) in μM, acquired docking parameters are provided in Table 10 under the best four conformers.

Table (11-A) shows the triple structure of the enzyme, the structure of the L^a ligand, and the method of attachment of the different positions of the L^a ligand within the active site of the enzyme, arranged from the highest binding energy to the lowest binding energy. The number and type of hydrogen bonding appear in the figure with amino acids for the active site. Where Table (11-A) shows the first position with the highest binding energy, the first generated conformer, and the binding of the ligand with two hydrogen bonds. The first bond is between hydrogen atom of bond donor and oxygen atom of amino acid Cysteine, which has a sequence of 300.

As for the L^b ligand, Table (11-B) shows the composition of the triple enzyme and the composition of the ligand, as well as the binding to the different positions within the active site from the highest binding energy to the lowest binding energy. It is noted from the figure that the ligand (the highest preferred position) binds to the active site with three hydrogen bonds. The first bond is between hydrogen atom of amino acid Serine and oxygen atom of the ligand, the second bond is between nitrogen atom of the amino acid Glutamine and the nitrogen atom of the ligand, and the third bond is between the hydrogen atom of the amino acid Threonine and oxygen atom of the ligand.

Table (10) shows the results of the docking study for ligands L^b and L^a, where the table shows a number of values obtained from the program, including the binding energy and the inhibition constant Intermolecular energy, as well as the number and type of hydrogen bonding.

For ligand L^a, the binding energy of the most favored position was equal to Kcal mol^{-1} -8.98, with an internal energy equal to Kcal/mol -12.26. Correlation study showed that the inhibition constant for the enzyme is 262.92 x 10^{-3} micromolar. Correlation values for

the rest of the modes can be seen in the table. For ligand L^4, the best binding position showed a binding energy of -7.16 Kcal/mol with an internal energy of Kcal mol^{-1} -11.64, while the inhibition constant was equal to 5.64 micromolar. It appears through the docking study results, Table (10), that the L^a ligand binds better with the active site of the enzyme than the L^b ligand, and is expected to show the highest effect against microbes [47-48].

Table (10): Docking parameters of potent discovered hits (L^a, L^b)

Comp. No.	Conformers	Binding Energy (Kcal mol-1)	Inhibition constant (μM)	Inter-molecular energy ($kcalmol^{-1}$)	H-bonds	Bonding
L^a	1	-8.98	262.92 X 10^{-3}	- 12.26	2	LIG:H:CYS300:O GLY301:HN:LIG:O
	2	-8.66	445.39 X 10^{-3}	- 11.95	1	THR 302:HN:LIG:O
	3	-7.56	2.88	- 10.84	1	SER303:HN:LIG:O
	4	-7.18	5.48	- 10.46	2	LIG:H:THR 352:OG1 GLY301:HN:LIG:O
	5	-6.46	18.27	- 9.75	1	VAL605:HN:LIG:O
	6	-5.79	57.37	- 9.07	2	LIG:H:ASP 354:OD 2 ALA602:HN:LIG:O
	7	-5.63	75.03	- 8.91	2	ALA602:HN:LIG:O VAL605:HN:LIG:O
	8	-5.60	79.05	- 8.88	2	LIG:H: ALA602:O GLY301:HN:LIG:O
	9	-4.81	297.46	- 8.09	0	-
	10	-4.75	327.26	- 8.04	1	ALA602:HN:LIG:O
L^b	1	-7.16	5.64	- 11.64	3	SER604:HN:LIG:O GLN 348:NH:LIG:N THR 352:HG1:LIG:O
	2	-6.97	7.83	- 11.44	2	LIG:H: ALA602:O THR 352:HG1:LIG:O
	3	-6.80	10.30	- 11.82	3	SER401:HN:LIG:O SER303:HN:LIG:O LIG:H: ALA602:O
	4	-6.78	10.74	- 11.25	3	SER401:HG:LIG:O LYS603:HZ3:LIG:N SER349:HN:LIG:O
	5	-5.96	42.72	- 10.44	2	SER 401:HN:LIG:O SER401:HG:LIG:O
	6	-5.18	160.31	- 9.65	1	SER 401:HG:LIG:O
	7	-5.14	172.01	- 9.61	0	-
	8	-4.83	289.84	- 9.30	1	THR302:HN:LIG:N,O
	9	-4.43	570.16	- 8.90	1	GLY301:HN:LIG:O
	10	-3.81	1.61 X 10^3	- 8.28	1	LIG:H: GLU488:OE2

Table (11-A): The docking of best generated conformers of potent discovered hits (L^a)

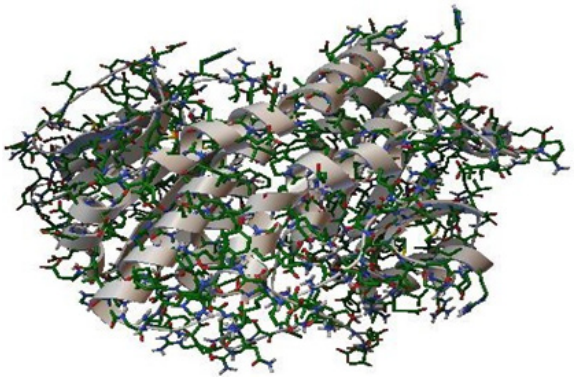	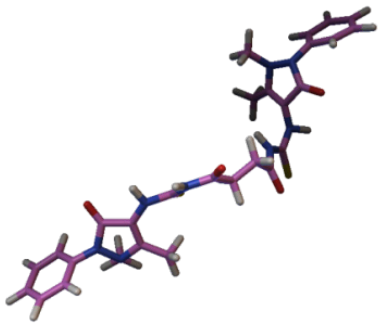
3-D structure of glucoseamine-6-phosphate (synthase (GlcN-6-p	Structure of compound ligand L^a
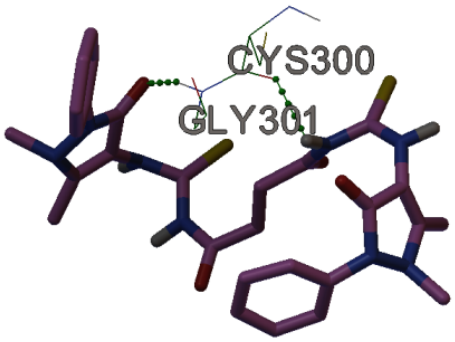	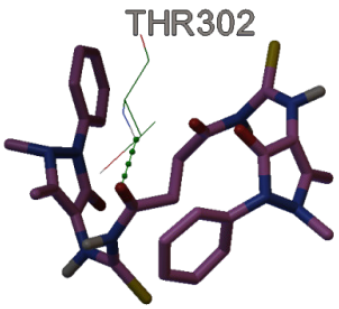
The first generated conformer of ligand L^a inside binding pocket of enzyme	The second generated conformer ligand L^a inside the binding pocket of enzyme
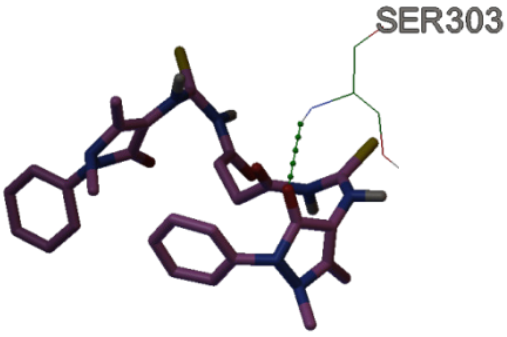	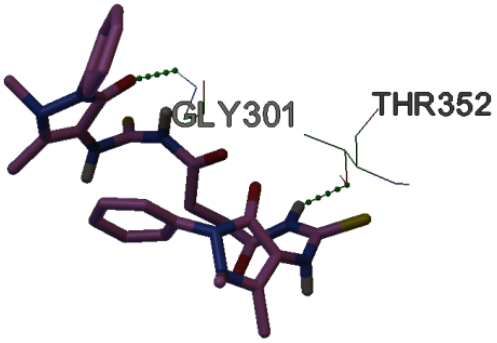
The third generated conformer of ligand L^a inside binding pocket of enzyme	The forth generated conformer of ligand L^a inside binding pocket of the enzyme

Table (11-B): The docking of best generated conformers of potent discovered hits (L^b)

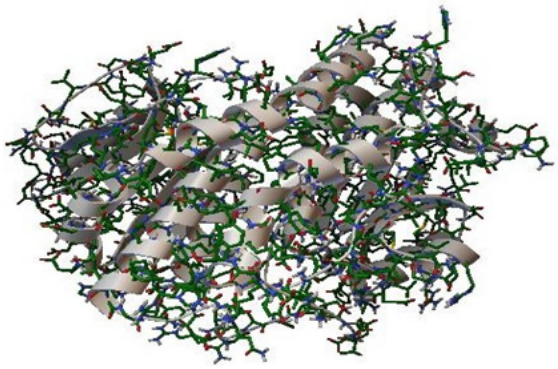	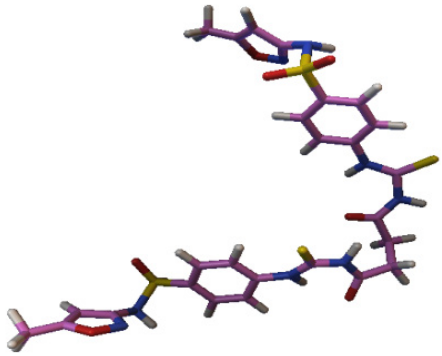
3-D structure of GlcN-6-p synthase	Structure of compound ligand ligand L^b
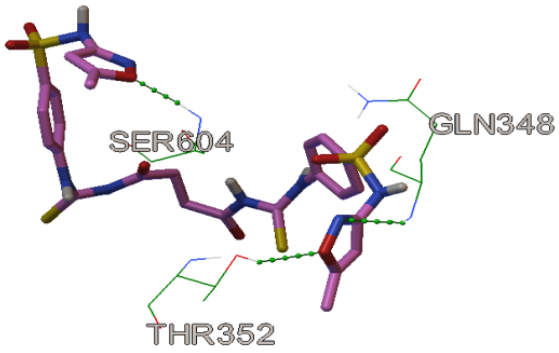	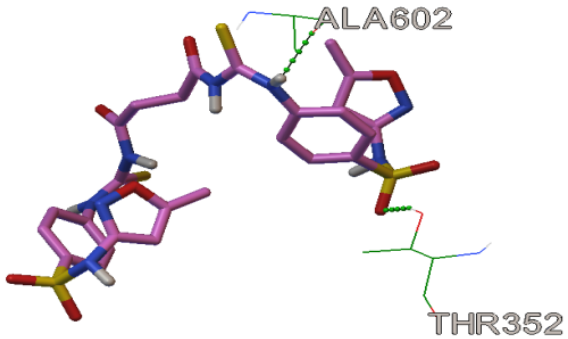
The first generated conformer of ligand L^b inside binding pocket of the enzyme	The second generated conformer of ligand L^b inside binding pocket of the enzyme
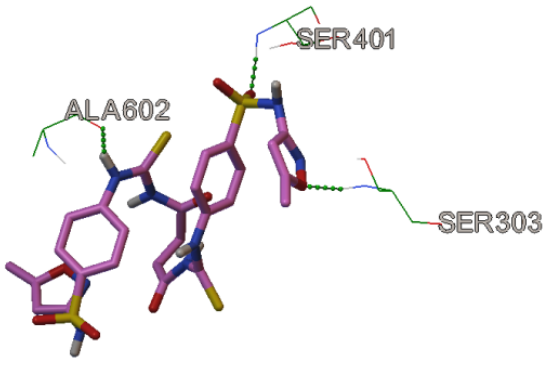	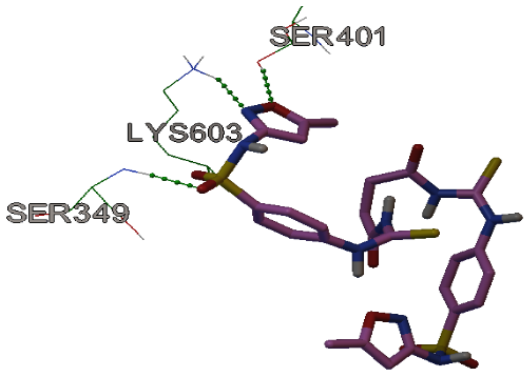
The third generated conformer of ligand L^b inside binding pocket of enzyme	The forth generated conformer of ligand L^b inside binding pocket of the enzyme

4. Conclusions

In the current investigation, transition metal ions, such as Ni (II), Mn (II), Cu (II), Co (II), Zn (II), Cd (II), and Hg (II) were used in the reactions of succinyl chloride with 4-aminoantipyrine and SMX to produce seven complexes of each ligand (L^a and L^b). The (C=S) and (C=O) groups were discovered to be the ligands (L^a and L^b) that were bidentate and potent donors. The anti-microbal activity of (L^a and L^b) and their complexes against two different species of bacteria were investigated. Using DPPH screening, the radical scavenging effectiveness of [Zn2(La)Cl4] and [Ni2(La)Cl4] was examined. The inclusion of -NH-C=S- functional groups and electron donating compounds both have a considerable impact on the radical scavenging efficacy of complexes, according to anti-oxidant measurements from attended compounds.

All of the investigated microbial species had GlcN-6-P synthase as their molecular target. Thus, for examining their virtual affinities and modes of binding with the enzyme, a number of the most powerful compounds (L^a,L^b) have been docked in a GlcN-6-P synthase model. The docked inhibitors (L^a,L^b) were discovered to bind to the orthosteric active site of the enzyme, suggesting that the investigated compounds may have a competitive inhibition binding mechanism. In conclusion, the recently created ligands may be effective leads for the creation of new anti-microbial agents.

Acknowledgement:

The College, its illustrious professors, and the laboratory staff deserve the authors' profound gratitude and admiration for helping to conduct all research measurements.

References

1. Xing Wang, et al., Synthesis and Antibacterial Activity Evaluation of Biphenyl and Dibenzofuran Derivatives as Potential Antimicrobial Agents against Antibiotic-Resistant Bacteria, Curr. Issues Mol. Biol. 2022, 44, 4087–4099.
2. Eman H. Al-Thubaiti , et al., Synthesis, Spectroscopic, Chemical Characterizations, Anticancer Capacities against HepG-2, Antibacterial and Antioxidant Activities of Cefotaxime Metal Complexes

with Ca(II), Cr(III), Zn(II), Cu(II) and Se(IV) ,Antibiotics 2022, 11, 967,1-24.

3. Chanat Chokejaroenrat , Chainarong Sakulthaew and Khomson Satchasataporn Enrofloxacin and Sulfamethoxazole Sorption on Carbonized Leonardite: Kinetics, Isotherms, Influential Effects, and Antibacterial Activity toward S. aureus ATCC 25923 , Antibiotics ,2022, 1261(11) ,1-22
4. Monther Faisal Mahdi , Rafah Fadhil Al-Smaism, Zainb Mohammed Abd Al-Khaliq, Synthesis, Characterization and antibacterial activity of new series of sulfamethoxazole derivatives, world journal of pharmacy and pharmaceutical sciences,2015, Vol. 4(10), 284-293.
5. Mostafa M. Ghorab , Marwa G. El-Gazzar and Mansour S. Alsaid , Synthesis, Characterization and Anti-Breast Cancer Activity of New 4-Aminoantipyrine-Based Heterocycles , Int. J. Mol. Sci. 2014, 15, 7539-7553.
6. Nnamdi C. Okey , Nnamdi L. Obasi and Paul M. Ejikeme, Evaluation of some amino benzoic acid and 4-aminoantipyrine derived Schiff bases as corrosion inhibitors for mild steel in acidic medium: Synthesis, experimental and computational studies, Journal of Molecular Liquids,2020, Vol.315, 113-773.
7. Basima M. Sarhan, Sajid M. Lateef and Enass J. Waheed, Synthesis and Characterization of Some Metal Complexes of [N-(1,5-dimethyl-3-oxo-2-phenyl-2,3-dihydro-1H-pyrazol4-ylcarbamothioyl) acetamide] , Ibn Al-Haitham Journal For Pure And Applied Science, 2015, 28(2) ,102-115.
8. Basima M. Sarhan ,Nada J. Kadhim and Enass J. Wheed, Stability constant of some Metal Ion Complexes of (6-(2- Amino-2-(4-hydroxy phenyl)-acetamido)-3,3- -dimethyl-7- oxo-4-thia-1-aza-bicyclo[3,2,0]heptanes-2- carboxylicacid (Amoxicillin), Ibn Al-Haitham Journal For Pure And Applied Science ,2013,vol. 26 (3) ,p.245-253.
9. Perihan A. Khalaf-Alla ,Antioxidant, Antimicrobial and Antitumor Studies of Transition Metal Complexes Derived from N-(2-Aminoethyl)-1,3-Propanediamine with DFT Calculations and Molecular

Docking Investigation ,Appl Organometal Chem. 2020;e5628.

10. Zabiulla , Salma Kouser, Molecular docking, synthesis and antimicrobial evaluation of metal complexes with Schiff base, Results in Chemistry, Volume 5, January 2023, 100650.
11. Awf A.R. Ahmed and Enass J. Waheed, "Synthesis, Characterization, Thermal Study, Biological Activity and Corrosion Inhibition of New Ligand Derived from Butanedioyl Dichloride and Some Selective Transition Metal Complexes" *Journal of Global Pharma Technology*(2019):vol11.pp379-391.
12. Taghreed Q. Abd Alkareem and Enass J. Waheed, Formation, Characterization and Antioxidant Study of Mixed Ligand Complexes Derived from Succinyl Chloride ,chem.methodol. 2022,6(12),914-928.
13. Shoaib, Mohammad, et al. "Synthesis of 4-aminoantipyrine derived Schiff bases and their evaluation for antibacterial, cytotoxic and free radical scavenging activity." Bangladesh Journal of Pharmacology 10.2 (2015): 332-36.
14. Alias, Mahasin F., Maysoon M. Abdul Hassan, and Sameaa J. Khammas. "Synthesis, characterization of some metal complexes with mixed ligands derived from sulfamethoxazole and 4, 4-dimethyl-2, 2-bipyridyl." Int. J. Sci. Res 4 (2015): 2337-2342.
15. Wagaa, Al, Fatima Ali, and Sahbaa Ali Ahmed. "Metal Pharmacologically Active Agents: Mode of New Tridentate Glycine amino acid with diketone (Benzil) and 4-Amino antipyrine Complexes." Egyptian Journal of Chemistry 65.5 (2022): 1-2.
16. Chaulia, S. N. "Metal complexes of multidentate azo dye ligand derived from 4-aminoantipyrine and 2, 4-dihydroxybenzoic acid; synthesis, characterization and biological activity." Der Pharma Chemica 8 (2016): 254-272.
17. El-Saied, Fathy A., Rafaat M. Issa, and Elsayeda A. Amerah. "Metal Complexes of Some Azo-and Azomethine Derivatives of Sulfamethoxazole." Smart Nanocomposites 2.2 (2011): 93.
18. Sahua, Nilima, et al. "Functionalized sulfamethoxazole and its

metal complex: Structural characterization, antibacterial and anticancer study of sulfamethoxazolyl-azo-salicylic acid and its copper (II) complex." J. Indian Chem. Soc97 (2020): 1199-1209.
19. Kurdekar, Gurunath S., et al. "4-Aminoantipyrine-based Schiff-base transition metal complexes as potent anticonvulsant agents." Medicinal Chemistry Research (2012),21: 2273-2279.
20. Hussein, Kawther Adeeb, Shatha Mahdi, and Naser Shaalan. "Synthesis, Spectroscopy of New Lanthanide Complexes with Schiff Base Derived From (4-Antipyrinecarboxaldehyde with Ethylene Di-Amine) and Study the Bioactivity." Baghdad Science Journal (2022): 0305-0305.
21. Ektirici, Sisem, et al. "Computational investigation of the monomer ratio and solvent environment for the complex formed between sulfamethoxazole and functional monomer methacrylic acid." ACS omega7.20 (2022): 17175-17184.
22. El-Saied, Fathy A., Rafaat M. Issa, and Elsayeda A. Amerah. "Metal Complexes of Some Azo-and Azomethine Derivatives of Sulfamethoxazole." Smart Nanocomposites 2.2 (2011): 93.
23. AbouEl-Enein, Saeyda A., et al. "Synthesis and characterization of some metal complexes derived from azo compound of 4, 4′-methylenedianiline and antipyrine: evaluation of their biological activity on some land snail species." Journal of Molecular Structure (2015), 1099: 567-578.
24. Alias, Mahasin F., Maysoon M. Abdul Hassan, and Sameaa J. Khammas. "Synthesis, characterization of some metal complexes with mixed ligands derived from sulfamethoxazole and 4, 4-dimethyl-2, 2-bipyridyl." Int. J. Sci. Res 4 (2015): 2337-2342.
25. K. Mohanan; C.J. Athira and Y. Sindhu . Synthesis, spectroscopic characterization and thermal studies of some lanthanide(III) nitrate complexes with a hydrazo derivative of 4-aminoantipyrine ,(2009), 27(5), 705–710.
26. Mohammed, H. J., and A. A. Syhood. "Spectrophotometric, thermal and determination of trace amount of palladium (II) nickel (II)

and silver (I) by using pyrazolone azo derivative." J Anal Pharm Res 7.4 (2018): 504-511.

27. Khan, Shabnam, et al. "Utilization of renewable waste material for the sustainable development of thermally stable and biologically active aliphatic amine modified Cardanol (phenolic lipid)-Formaldehyde free standing films." Journal of Cleaner Production 196 (2018): 1644-1656.
28. Abdul-Hassan, Maysoon M., and Nibal Kh Mousa. "Antimicrobial activity of new transition metal complexes of sulfamethoxazole on nhibiter by Staphylococcus aureus, Pseudomonas aeruginosa, Salmonella typhi and Escherichia coli." AIP Conference Proceedings. 2020,Vol. 2290. No. 1. pp.23-34
29. Joseph, Renjini, and K. Girish Kumar. "Differential pulse voltammetric determination and catalytic oxidation of sulfamethoxazole using [5, 10, 15, 20-tetrakis (3-methoxy-4-hydroxy phenyl) porphyrinato] Cu (II) modified carbon paste sensor." Drug testing and analysis 2.6 (2010): 278-283.
30. Masters, Philip A., et al. "Trimethoprim-sulfamethoxazole revisited." Archives of internal medicine 163.4 (2003): 402-410.
31. Teran, Rommy, et al. "Characterization of antimicrobial, antioxidant, and leishmanicidal activities of Schiff base derivatives of 4-aminoantipyrine." Molecules 24.15 (2019): 2696.
32. El-Nawawy, M. A., et al. "Synthesis, spectroscopic, thermal studies and biological activity of a new sulfamethoxazole schiff base and its copper complexes." Int J Pharm Sci Res 2.12 (2011): 3143-3148.
33. Hadi Kadhim, S., and Qahtan Abd-Alla. "I, Jawad Hashim T. Synthesis and Characteristic Study of Co (II), Ni (II) And Cu (II) Complexes of New Schiff Base Derived from 4-Amino Antipyrine." Int J Chem Sci 15.1 (2017): 107.
34. Agarwal, Ram K., Lakshman Singh, and Deepak Kumar Sharma. "Synthesis, spectral, and biological properties of copper (II) complexes of thiosemicarbazones of Schiff bases derived from 4-aminoantipyrine and aromatic aldehydes." Bioinorganic Chemistry and Applications 2006 (2006).

35. Tyagi, Monika, et al. "Synthesis, characterization and anti-fungal evaluation of Ni (II) and Cu (II) complexes with a derivative of 4-aminoantipyrine." Journal of Taibah University for Science 11.1 (2017): 110-120.
36. Habila, Imane, et al. "A new complex of Zinc (II) with sulfamethoxazole ligand: Synthesis, crystal structure, Hirshfeld surface analysis, thermal properties, DFT calculations and antibacterial/antifungal activities." Journal of Molecular Structure 1244 (2021): 130903.
37. Mahdi, Raheem Taher, Taghreed H. Al-Noor, and Ahmed H. Ismail. "Preparation, characterization, and antibacterial properties of mixed ligand complexes of L-leucine and Sulfamethoxazole with Mn (II), Co (II), Ni (II), Cu (II), Zn (II), Cd (II) and Hg (II) ions." Advances in Physics Theories and Applications 27 (2014): 8-19.
38. Kesimli, B., and A. Topacli. "Infrared studies on Co and Cd complexes of sulfamethoxazole." Spectrochimica Acta Part A: Molecular and Biomolecular Spectroscopy 57.5 (2001): 1031-1036.
39. Willis J. B. and Mellor D. P., The Magnetic Susceptibility of Some Nickel Complexes in Solution, J. Am. Chem. Soc. (1947), 69, 6, 1237–1240.
40. Revanasiddappa, M. , et al, Electrical Conductivity Studies on Co(II), Cu(II), Ni(II) and Cd(II) Complexes of Azines ,Journal of Chemistry , Vol. 5, No.4, pp. 797-801, 2008.
41. Bozza, G., et al., Claudia, Eduardo Tonon . Synthesis and thermal behavior study of complexes of the type $[Pd(\mu\text{-}X)(4\text{-eb-p-phen})]_2$ (X = Cl, Br, I, N_3, NCO, SCN) and 4-eb-p-phen [bis(4-ethylbenzyl) p-phenylenediimine]. Journal of Thermal Analysis and Calorimetry, (2014) 118(1), 67–74.
42. Wenkin, M., et al. "Diammine (pyrazine-2, 3-dicarboxylato-N, O) palladium (II): synthesis , crystal structure, spectroscopic and thermal properties." Inorganica chimica acta 258.1 (1997): 113-118.
43. Juber, A. , et al. "Design, Synthesis, Characterization and Biological Evaluation of 6-Methoxy-2-aminobenzothioate derivatives against certain bacterial strains." Egyptian Journal of Chemistry 63.10 (2020):

3891-3901.

44. Khalil, M. , and Khalal. Q. "Synthesis and characterization of new compounds derived from 2-hydrazinobenzothiazole and evaluated their antibacterial
45. choudhary, alka; sharma, renu; nagar, meena; mohsin, mohammed; meena, har sahay (2011). Synthesis, Characterization and Antioxidant activity of some transition metal complexes with terpenoid derivatives. journal of the chilean chemical society, 56(4), 911–917.
46. Esteban Rodríguez-Arce , Marianela Saldías, Antioxidant properties of flavonoid metal complexes and their potential inclusion in the development of novel strategies for the treatment against neurodegenerative diseases, Biomedicine & Pharmacotherapy,Volume 143, November 2021, 112236
47. Zabiulla , Salma Kouser, Molecular docking, synthesis and antimicrobial evaluation of metal complexes with Schiff base, Results in Chemistry, Volume 5, January 2023, 100650.
48. Ammar, Yousry A., et al. "Design, synthesis, antiproliferative activity, molecular docking and cell cycle analysis of some novel (morpholinosulfonyl) isatins with potential EGFR inhibitory activity." European journal of medicinal chemistry 156 (2018): 918-932.